Statistical distribution of mirror mode-like structures in the magnetosheaths of unmagnetised planets: 2. Venus as observed by the Venus Express spacecraft

Martin Volwerk[1], Cyril Simon Wedlund[1], David Mautner[1], Sebastián Rojas Mata[2], Gabriella Stenberg Wieser[2], Yoshifumi Futaana[2], Christian Mazelle[3], Diana Rojas-Castillo[4], César Bertucci[5], and Magda Delva[1]

[1]Austrian Academy of Sciences, Space Research Institute, Graz, Austria
[2]Swedish Institute of Space Physics, Kiruna, Sweden
[3]Institut de Recherche en Astrophysique et Planétologie (IRAP), Université de Toulouse, CNRS, UPS, CNES, Toulouse, France
[4]Instituto de Geofísica, Universidad Nacional Autónoma de México, Coyoacán, Mexico
[5]Instituto de Astronomía y Física del Espacio, Ciudad Autónoma de Buenos Aires, Argentina

Correspondence: Martin Volwerk (martin.volwerk@oeaw.ac.at)

Abstract. In this series of papers, we present statistical maps of mirror mode-like (MM) structures in the magnetosheaths of Mars and Venus and calculate the probability of detecting them in spacecraft data. We aim to study and compare them with the same tools and a similar payload at both planets. We consider their dependence on Extreme Ultraviolet (EUV) solar flux levels (high and low).

5   The detection of these structures is done through magnetic field-only criteria and ambiguous determinations are checked further. In line with many previous studies at Earth, this technique has the advantage of using one instrument (a magnetometer) with good time resolution facilitating comparisons between planetary and cometary environments.

    Applied to the magnetometer data of the Venus Express (VEX) spacecraft from May 2006 to November 2014, we detect structures closely resembling MMs lasting in total more than $93,000$ s, corresponding to about 0.6% of VEX's total time spent

10   in the Venus's plasma environment. We calculate MM-like occurrences normalised to the spacecraft's residence time during the course of the mission. Detection probabilities are about 10% at most for any given controlling parameter.

    In general, MM-like structures appear in two main regions, one behind the shock, the other close to the induced magnetospheric boundary, as expected from theory. For solar maximum, the active region behind the bow shock is further inside the magneosheath, near the solar minimum bow shock location. The ratios of the observations during solar minimum and maxi-

15   mum are slightly dependent on the depth $\Delta B/B$ of the structures, deeper structures are more prevalent at solar maximum. A dependence on solar EUV (F10.7) flux is also present, where at higher F10.7 flux the events occur at higher values than the daily average value of the flux. Combining the plasma data from the Ion Mass Analyser with the magnetometer data shows that the instability criterion for MMs is reduced in the two main regions where the structures are measured, whereas it is still enhanced in the region in-between these two regions, implicating that the generation of MMs is transferring energy from the

20   particles to the field.

This study is the second of two on the magnetosheaths of Mars and Venus, and a third paper comparing the results obtained at the two planets will follow.

1 Introduction

Mirror modes (MMs) are ubiquitous structures in space plasmas, which consist of trains of magnetic depressions combined
25 with plasma density enhancements in anti-phase. They are stationary in the plasma frame and convect with the plasma flow. Most often, these structures are found in planetary magnetosheaths, behind a quasi-perpendicular bow shock. MMs have been found at Earth (e.g., Tsurutani et al., 1982; Baumjohann et al., 1999; Lucek et al., 1999a; Soucek et al., 2015), Venus (e.g., Bavassano Cattaneo et al., 1998; Volwerk et al., 2008a, b; Schmid et al., 2014; Volwerk et al., 2016), Mars (e.g., Bertucci et al., 2004; Espley et al., 2004; Simon Wedlund et al., 2022a), Jupiter (e.g., Erdös and Balogh, 1996; Joy et al., 2006), Saturn (e.g.,
30 Bavassano Cattaneo et al., 1998), and comets (e.g., Mazelle et al., 1991; Glassmeier et al., 1993; Schmid et al., 2014; Volwerk et al., 2014).

MMs are created by a temperature asymmetry in the plasma, where the perpendicular temperature, $T_\perp$ (with respect to the magnetic field) is higher than the parallel temperature, $T_\parallel$. Hasegawa (1969) showed that for a bi-Maxwellian plasma the instability criterion is given by:

35 $$\text{MMI} = 1 + \sum_i \beta_{i\perp} \left(1 - \frac{T_{i\perp}}{T_{i\parallel}} \right) < 0, \tag{1}$$

where

$$\beta_{i,\perp} = \frac{n_i k_\text{B} T_{i\perp}}{B^2/2\mu_0}, \tag{2}$$

is the perpendicular plasma-β of species i, the ratio of perpendicular (to the magnetic field) plasma pressure and the magnetic pressure. Here n_i is the density of species i, k_B is Bolzmann's constant and μ_0 is the permeability of vacuum.

40 This temperature asymmetry can give rise to two different instabilities: the (Alfvén) ion cyclotron instability for low-β plasma, and the mirror mode instability for high-β plasma (Gary, 1992; Gary et al., 1993). Southwood and Kivelson (1993) defined the instability criterion, for protons p only, as $R_\text{SK} > 1$, where:

$$R_\text{SK} = \frac{T_{p,\perp}/T_{p,\parallel}}{1 + 1/\beta_{p,\perp}} \tag{3}$$

The increase in the perpendicular temperature or pressure can be created in various ways, which may be concurrent in
45 the plasma: through pick-up, where the newly created ion starts gyrating around the magnetic field; through perpendicular energization whilst crossing the quasi-perpendicular bow shock; and through slow changes in B strength with conservation of first adiabatic invariant. The first process will occur mainly in the solar wind interaction with the planetary exosphere (with the

exception of Jupiter's magnetosphere and the Galilean moons, where the Jovian corotating magnetic field and magnetospheric plasma is taking the role of the solar wind) in the low-β plasma case and generation of ion cyclotron waves will take place

50 (Delva et al., 2008, 2009, 2011, 2015; Schmid et al., 2021).

The temporal evolution of MMs, while they are convected with the plasma flow, has been discussed by Hasegawa and Tsurutani (2011). It is assumed that there is a Bohm-like diffusion (Bohm et al., 1949) taking place in the MM structures, where the higher frequencies of the structure diffuse faster than the lower ones, and thereby the MMs grow in size. This phenomenon was shown to occur at Venus and at comet 1P/Halley (Schmid et al., 2014).

55 The temperature asymmetry of the plasma is an important factor in the generation of MMs. Lately, the data of the Ion Mass Analyser (IMA) of the ASPERA-4 instrument (Barabash et al., 2007) have been re-evaluated and reprocessed by Bader et al. (2019), with special interest to deduce the proton temperatures, $T_\parallel$ and $T_\perp$. This resulted in maps displaying, amongst others, the temperature asymmetry necessary for the MM instability criterion in Eq. (1). It also showed that mainly in the "near-subsolar magnetosheath" there was a large ratio of $T_\perp/T_\parallel \approx 1.56$, whereas in other regions this ratio was ~ 1.

60 Rojas Mata et al. (2022) extended this study and also took into account the possible differences between solar minimum and maximum conditions. They found that $T_\parallel$ and $T_\perp$ are 20 to 35% lower during solar maximum as compared with solar minimum. However, the ratio $T_\perp/T_\parallel$ does not change, but the regions with a higher anisotropy are found further away from the bow shock during solar maximume conditions.

In this paper we make a statistical study of the Venus Express (VEX, Svedhem et al., 2007) mission magnetometer (VEX-65 MAG, Zhang et al., 2006) data. In a companion paper by Simon Wedlund et al. (2022b, Paper 1) a similar study using the same detection criteria for MM-like structures is done with the MAVEN data at Mars.

2 Detecting mirror mode-like structures in spacecraft data

2.1 Instrumentation

VEX was brought into a polar orbit around Venus in 2005 with an elliptical orbit and periapsis at ~ 300 km from the surface, 70 which means the spacecraft entered well into the induced magnetosphere. The VEXMAG data used here have a sampling rate of 1 Hz, but are also available at 32 Hz (and for short intervals a sampling rate of 128 Hz exists). However, as the MM structures have a period of $4 \leq T_{\mathrm{mm}} \leq 15$ s (Volwerk et al., 2008a, b, 2016) the 1 Hz data are sufficient. Unfortunately, the dats from the Ion Mass Analyzer (IMA) of the ASPERA-4 instrument (Barabash et al., 2007) only has a resolution of 192 s for ions, which means that these data can only give us a indication of the plasma conditions (see e.g. Bader et al., 2019; Rojas Mata et al., 75 2022).

In this paper the full dataset over the VEX mission period is used, from May 2006 to November 2014, which contains both a solar minimum and solar maximum period as is shown in Fig. 1 (see also Delva et al., 2015; Volwerk et al., 2016). In this way there can be a comparison between the probability and location of MM-like structures in either solar activity period.
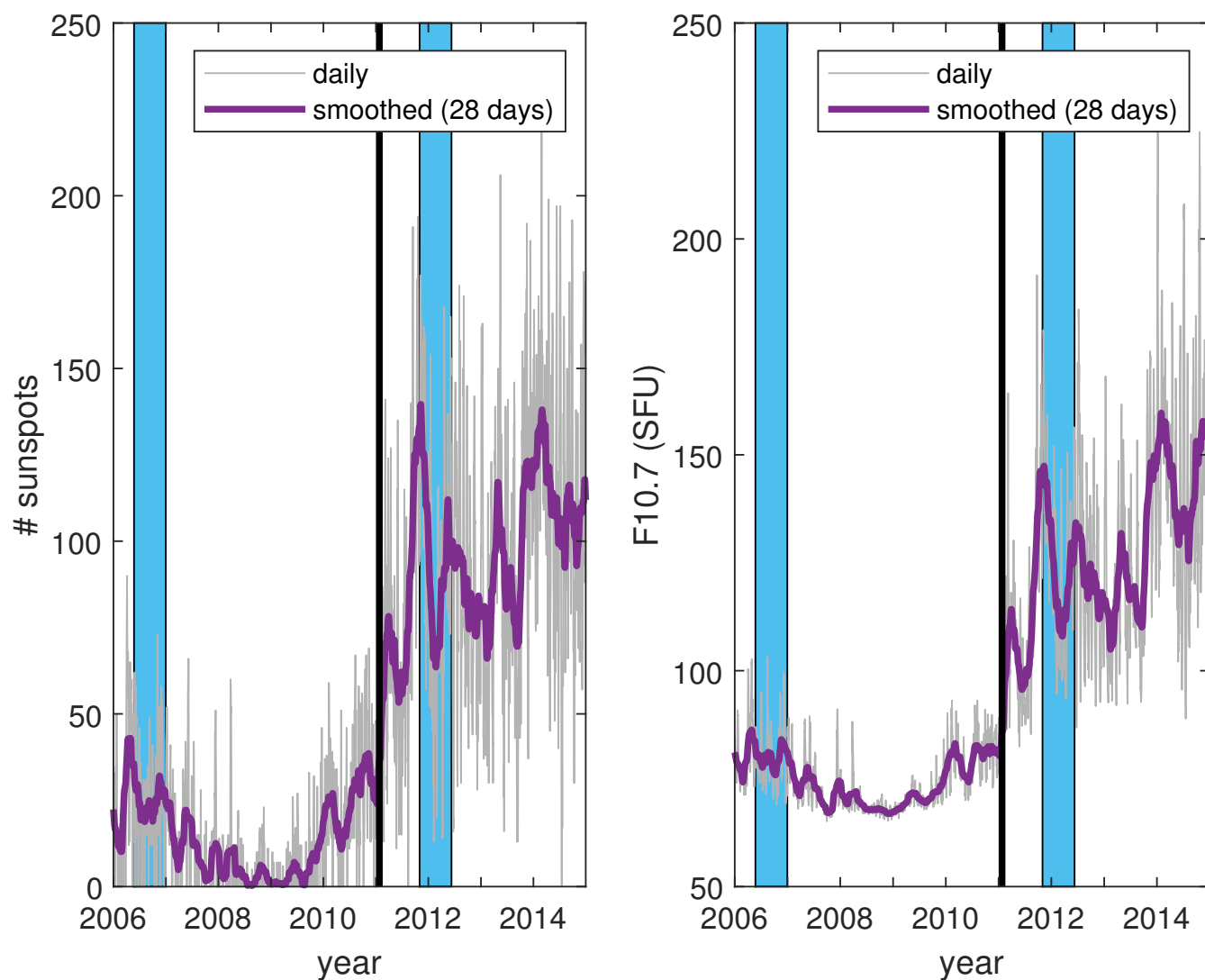
Figure 1. The daily (grey) sunspot numbers (left) and F10.7 flux (right) over the duration of the VEX mission (2006 - 2014) and the smoothed (over 28 days) numbers (red). The vertical line at 25 January 2011 is marking the (slightly arbitrary) boundary between the solar minimum and solar maximum periods, split at # sunspots = 50, or F10.7 = 100 SFU. The two blue boxes show the intervals discussed in Volwerk et al. (2016).

2.2 Detection method

2.2.1 B-field only criteria

In order to detect the MM-like[1] structures in the VEXMAG data we use the method introduced by Simon Wedlund et al. (2022a), which is slightly different, but more accurate, from that used by Volwerk et al. (2008a). Because of the lack of high-resolution ion data, the detection method is based on magnetic field measurements only. We take the same magnetic field-only criteria as in Table 1 of Paper 1. They are based on several previous works including Lucek et al. (1999a, b) and Volwerk et al. (2008a) and expanded on by Simon Wedlund et al. (2022a).

1. The data $\mathbf{B}$ are low-pass filtered with a two-minute-wide Butterworth filter to determine the background field $\mathbf{B}_{\mathrm{bg}}$, with $|\mathbf{B}_{\mathrm{bg}}| > 5$ nT to isolate magnetosheath conditions from average solar wind values;

2. From the data and the background field we calculate $\Delta|\mathbf{B}|/|\mathbf{B}_{\mathrm{bg}}| = (|\mathbf{B}| - |\mathbf{B}_{\mathrm{bg}}|)/|\mathbf{B}_{\mathrm{bg}}|^2$, where a threshold is set to $\Delta|\mathbf{B}|/|\mathbf{B}_{\mathrm{bg}}| \geq 0.15$;

3. Then we apply a Minimum Variance Analysis (MVA, Sonnerup and Scheible, 1998) on 15-s wide sliding windows with a 1-s shift, to obtain the directions of the minumum and maximum variations. A requirement on the maximum, minimum and intermediate eigenvalues is set to $\lambda_{\max}/\lambda_{\mathrm{int}} \geq 3$ and $\lambda_{\mathrm{int}}/\lambda_{\min} \leq 8$;

4. The angles between the minimum/maximum variation direction and the background magnetic field should be: $\Phi_{\mathrm{minV}} \geq 70°$ and $\Theta_{\mathrm{maxV}} \leq 20°$;

5. The azimuth $az = \arctan(B_y/B_z)$ and elevation $el = \arctan\left(B_z/\sqrt{B_x^2 + B_y^2}\right)$ of the magnetic field are caculated and for MM-like structures it is expected that the rotation of the magnetic field over the structure $\Delta(az, el) \leq 10°$.

The reasons of these choices above are explained in more detail in Paper 1, to which the reader is referred to.

2.2.2 Removal of false positive detections

In order to find when the spacecraft is in Venus's magnetosheath, the database of calculated bow shock crossings based on the models by Zhang et al. (2008) and Russell et al. (1988). A margin is set on the crossing times of ~ 30 min, which corresponds to 14400 km, or 2.3 R_{V}, to be sure we capture the true bow shock in the data.

We should note that around the bow shock there are other kinds of structures which have similer characteristics in polarization and compression as the MMs that we are looking for. These waves are also linked to pickup ion processes, in the case of the quasi-parallel shock. So looking at the magnetic field only, strong fluctuations ($\Delta|\mathbf{B}|/B_{\mathrm{bg}} \geq 0.1$) may appear, which are not sinusoidal and have a quasi-linear polarisation, without these structures necessarily being MMs. Most of the time, magnetic

---

[1]We use the term "MM-like" throughout the paper as the usage of magnetic field only methods does not unambiguously identify MMs, whichs is only possible with plasma data at an appropriate resolution.

[2]Note that there is a difference of a factor 2 compared to the papers by Volwerk et al.

field intensity and plasma density will typically be in phase, as opposed to the expected MM behaviour (Hasegawa, 1969). However, this information is sometimes neither available at the desired high time resolution (as in our case with VEX data) nor practical to derive as in large statistical surveys.

Two strategies can be made in order to exclude non-MM signatures: (1) making sure that the magnetic field across the structures' region does not rotate more than 10–20°, as theoretically predicted for MMs (Treumann et al., 2004) and in agreement with past observations (Tsurutani et al., 2011), and (2) restricting the detections to magnetosheath conditions only and excluding the region around the bow shock to avoid these foreshock transients.

Strategy (1) constrains the detected structures to behaviours more reminiscent of MMs: we apply criterion 5 listed in Sect. refsec:detection, which ensures that the magnetic field does not rotate significantly across the structure. From the magnetic field vector the magnetic azimuth and elevation angles are defined as:

$$az = \arctan\left(B_y/B_x\right) \tag{4}$$

and

$$el = \arctan\left(B_z/\sqrt{B_x^2 + B_y^2}\right) \tag{5}$$

First, we define "regions", which contain structures detected within a maximum of 30 s between one another and ignore isolated singular events; two separate regions are thus more than 30 s apart. This particular value of 30 s was chosen empirically as double the length of the longest MM structures found at Mars or Venus (see for example Simon Wedlund et al., 2022a; Volwerk et al., 2008b, 2016); moreover this ensures that rotations could be calculated for trains of MM-like structures for which the 2-min windowed background magnetic field values would be representative. We then estimate how much azimuth and elevation angles fluctuate at the detected position of the candidate structure by calculating their running standard deviation $\langle\sigma(az,el)\rangle$ over a 2-min sliding interval, keeping only those structures where $\langle\sigma(az,el)\rangle$ is less than 10° for each angle (Simon Wedlund et al., 2022a).

Complementarily, strategy (2) makes use of the position of the bow shock crossing in the spacecraft data and ignores the detected structures in a range of radial distances around it (or equivalently, in a range of durations around the time of the crossing).

For Mars the automatic bow shock predictor-corrector algorithm based on magnetic field measurements only was used, explained in Simon Wedlund et al. (2022a). This analys has not (yet) been done for Venus and thus this product does not exist. Therefore, only the first strategy has been applied in this paper.

2.2.3 Examples

Figure 2 shows a three-minute interval of VEXMAG data on 5 May 2006, where VEX is in Venus's magnetosheath (see also Volwerk et al., 2008b, Fig. 1), where the selection criteria by Volwerk et al. (2008a, grey) and by Simon Wedlund et al. (2022a, green) are compared. It is clear from most panels that both methods find the same values for most parameters. However, because of the extra restrictions the CSW-method identifies fewer, but therefore robuster, MM-like structures.
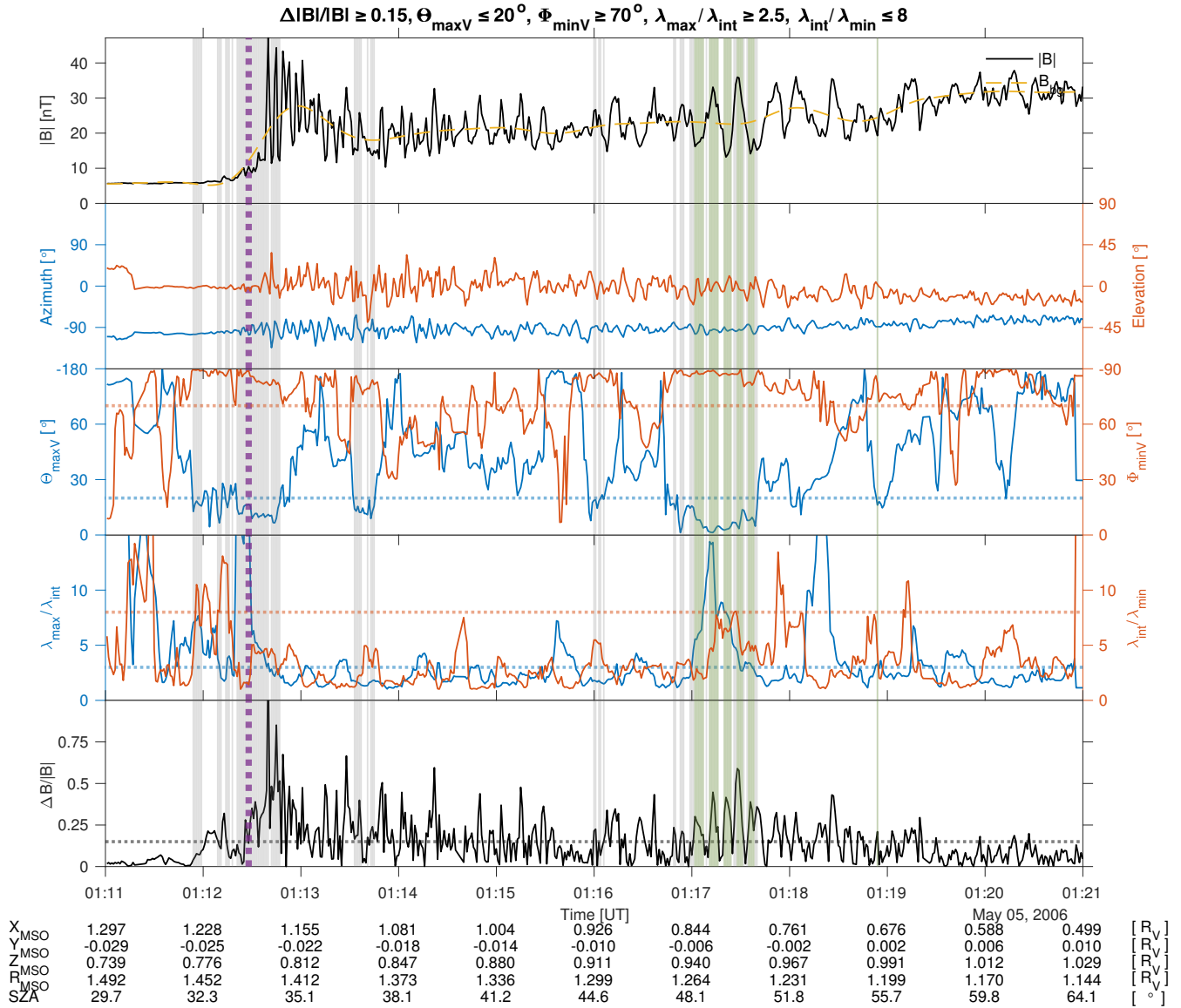
Figure 2. Ten minutes on 5 May 2006 when VEX entered through the bow shock into the magnetosheath. Shown are (a) The total magentic field; (b) The azimuth and elevation of the magnetic field; (c) The angles of the minimum and maximum variation direction with the background magnetic field; (d) the ratios of the eigen values and (e) the $\Delta B/B$. The grey shadings show the events found with the criteria in Volwerk et al. (2008a) and the green shadings show those found with the criteria in Simon Wedlund et al. (2022a) (with the green shading overlapping the grey shading). The purple vertical dotted line is the model-location of the bow shock.
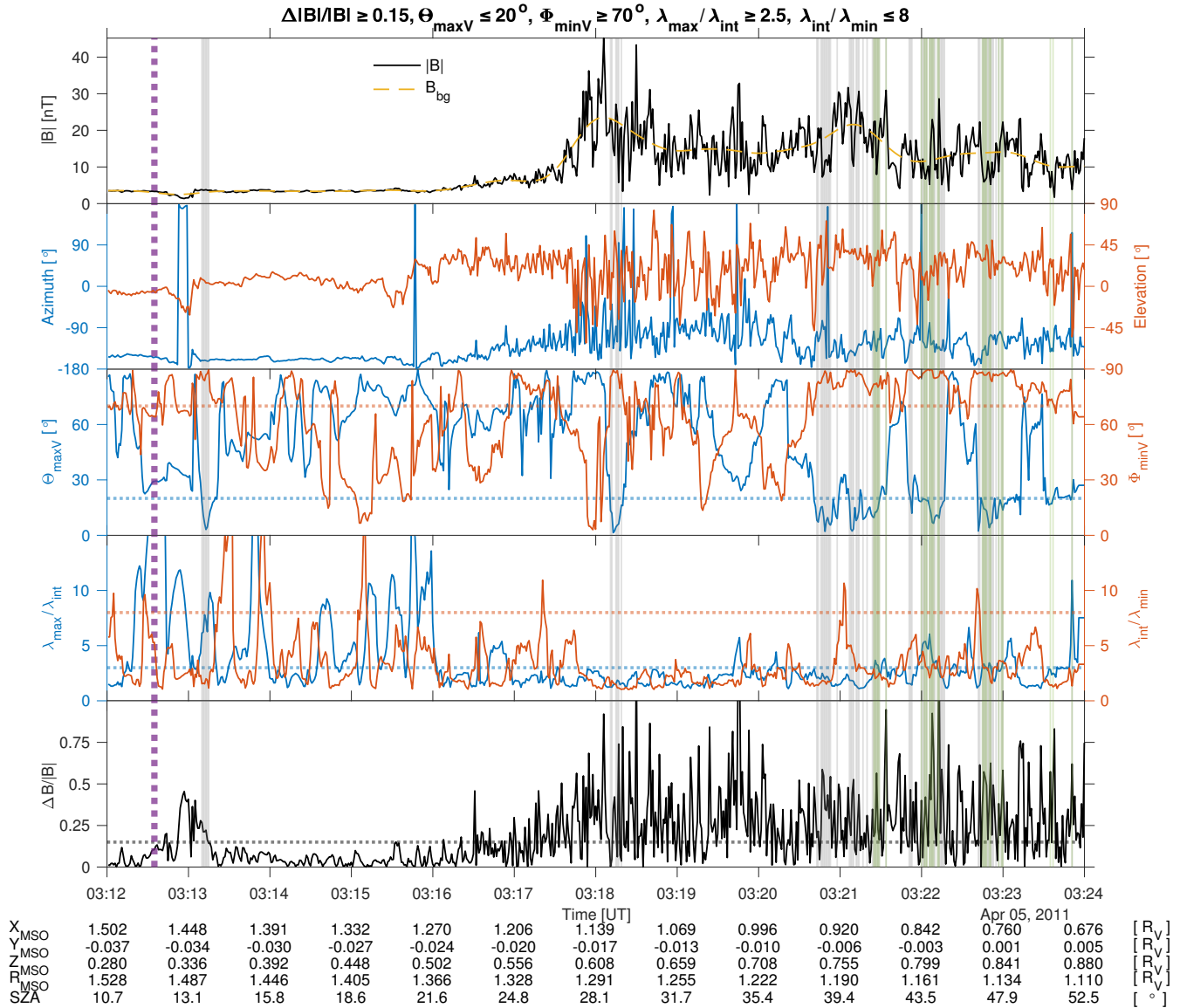
Figure 3. Twelve minutes on 5 April 2011 when VEX entered through the bow shock into the magnetosheath. Same format as Fig. 2. Clearly the model bow shock does not describe the true position well.

In Fig. 3 the inbound part of a solar maximum orbit of VEX is shown, where there are some determinations of MM-like structures close to the BS and further inside the magnetosheath.

Table 1. Total number of MM-like structures in the VEXMAG dataset (equivalent to a duration in s because of the magnetometer resolution of 1 s) and residence times, probability $\mathcal{P}$, and averaged MM depth $\langle \Delta B / B \rangle$ for solar minimum and maximum. For the total detections based only on Φ_{minV} and Θ_{maxV} (quasi-linearity of the structures), numbers in brackets.

period	Total MM-like structures	ΔT^{sc}	Probability	Average
	#	seconds	%	$\langle \Delta B / B \rangle$
		days		
Sol. Min.	38,901	8,441,391	~ 0.5	0.14 ± 0.12
	(164,418)	97.7	(~ 2)	
Sol. Max	54,883	7,611,965	~ 0.8	0.18 ± 0.20
	(213,234)	88.1	(~ 3)	

2.3 Mapping technique

Following the mapping technique of Paper I, the results are shown on a grid on cylindrical coordinates based on the VSO coordinate system[3], i.e. X_{VSO} and $R_{\mathrm{VSO}} = \sqrt{Y_{\mathrm{VSO}}^2 + Z_{\mathrm{VSO}}^2}$ with a size of $0.1 \times 0.1 \, R_{\mathrm{V}}$. For each grid cell the total number of seconds for which the MM criteria are fulfilled, $\Delta T^{\mathrm{struct}}$, is calculated as well as the total residence time of VEX in that box, ΔT^{sc}. Both determinations are done for solar minimum and solar maximum. The probability of MM-like structures is then simply calculated from the ratio of the two:

$$\mathcal{P} = \frac{\Delta T^{\mathrm{struct}}}{\Delta T^{\mathrm{sc}}}. \tag{6}$$

A first quick result can be obtained by looking at the total duration of MM-like structures spanning years 2004-2016 of VEXMAG data. as shown in Table 1. The total residence time shows that VEX was longer in the magnetosheath for solar minimum than for solar maximum. This is caused by the asymmetric division of the VEX mission (see Fig. 1) and is influenced by a change in attitude of the orbit over the duration of the mission, where the semi-major axis slowly rotated further southward and in the late stage of the mission back northward again. Nevertheless, more events are found and the total observational rate is $\sim 50\%$ higher during solar maximum. Note that, although these are both multiple years of orbits, the time spent in the magnetosheath is actually rather short, 185.8 days, because of the strongly elliptical orbit with a periapsis and apoapsis of 250 km ($1.04 \, R_{\mathrm{V}}$) and 66000 km ($11.90 \, R_{\mathrm{V}}$), respectively, whereas the magnetosheath spans typical radial distances of 1.1 to 1.5-3 R_{V}.

In Figs. 7 and 8 (left panels) the total residence time of the spacecraft in $0.1 \times 0.1 \, R_{\mathrm{V}}$ cells is shown for solar minimum and maximum. It shows that there is a slight difference of total residence times in e.g. the polar region, where VEX spent relatively less time during the solar maximum interval.

---

[3]VSO: Venus-Solar-Orbital coordinate system, where X_{VSO} points towards the Sun, Z_{VSO} is towards solar north and Y_{VSO} completes the triad and is in the opposite direction of Venus's orbit.

2.4 Calculating MM-like observational probability

160 The overall numbers and probabilities only give a small indication that MM-like structures are more prone to be excited during solar maximum as compared to solar minimum. The interesting part is when the probability per $0.1 \times 0.1\,R_{\mathrm{V}}$ cell is examined.

Figures 7 and 8 show the statistical results of our search for solar minimum and maximum respectively. The left panels show the total residence time ΔT^{sc} of VEX in each grid cell. The middle panel shows the probability of MM-like structures per cell calculated with Eq. (6). The right panel shows the mean $\langle \Delta B/B \rangle$ in each grid cell, limited by the restriction that 165 $\langle \Delta B/B_{\mathrm{bg}} \rangle \geq 0.15$.

There are clearly two regions on the dayside where the MM-like structures are most prevalent: for solar minimum right behind the BS and close to the ionopause, and for solar maximum also behind the bow shock, but slightly deeper inside the magnetosheath, and again at the magnetopause/ionopause. In a marginal way, there is also a third area behind the planet, around $(X, R) = (-2, 0)R_{\mathrm{V}}$, where MM-like structures seem to be present for solar maximum, which is not so prominent at 170 solar minimum. One may assume that the creation of the first two regions is caused by two anisotropic energization mechanisms of the ions: close to the bow shock the perpendicular temperature is enhanced by preferential heating along the perpendicular direction of ions crossing the quasi-perpendicular BS; close to the magnetopause/ionopause the perpendicular temperature is enhanced by the magnetic pile-up in front of the planet and the conservation of the first adiabatic invariant.

2.5 Controlling parameters

175 The presence of MM-like structures in Venus's magnetosheath is first of all dependent on the type of bow shock. A quasi-perpendicular bow shock has its normal nearly perpendicular to the impinging IMF. In this case the picked-up protons in the solar wind are energized mainly in the direction perpendicular to the magnetic field. This increases the $T_{\perp}/T_{\parallel}$ term in the instability criterion, Eq. (1), and thus MM-like structures are expected to be generated. However, this criterion is not sufficient condition, as was shown in the data from the Solar Orbiter flyby of Venus, where behind a near-perpendicular bow shock, 180 ion cyclotron waves (ICW) were generated (Volwerk et al., 2021) instead of MM-like structures. This was caused by a low plasma-$\beta (\approx 1.3)$ behind the bow shock. Gary et al. (1993) showed that, for low plasma-β, the ratio $T_{\perp}/T_{\parallel}$ must be $\sim 15\%$ larger for MM generation than for ICW generation.

Behind a quasi-parallel bow shock the generation of MM-like structures is not expected to be significant due to the lack of perpendicular energization of the protons, which was shown by Volwerk et al. (2008b). In this condition, pickup ion effects 185 alone may lead to temperature anisotropies able to generate MMs (Gary, 1992).

Venus's orbit has an excentricity of $\epsilon \approx 0.007$, which means that, unlike Mars with an eccentricity, $\epsilon \approx 0.0935$, seasonal effects are not expected. However, the bow shock location for solar minimum and maximum is significantly different. For example, the terminator distance is $R_{\mathrm{t,min}} \approx 2.14\,R_{\mathrm{V}}$ (Zhang et al., 2008) and $R_{\mathrm{t,max}} \approx 2.40\,R_{\mathrm{V}}$ (Russell et al., 1988): for solar maximum conditions, the bow shock significantly expands in the solar wind and inflates by more than 10%. The difference 190 between the two solar activities is clear through the further distance into the magnetosheath of the MM probability peak for solar maximum.

It should be noted, however, that the maximum of solar cycle 24 was (much) weaker then previous solar maxima (see e.g., McComas et al., 2013), which means that the solar wind conditions may not be representative of a "regular" solar maximum.

3 Results

3.1 Overview of the full dataset

In Fig. 4 we show the Probability Distribution Function (PDF) of all variables necessary in the selection criteria listed in Sect. 2.2, for the whole mission. The maxima of the PDFs have been indicated by a grey bar in the panels. These PDFs need to be checked against the selection criteria. Panels (b) through (f) show that for the largest part of the events the single selection criteria are indeed fulfilled, however, it is the combination of the five that need to work together to have a positive identification.

Putting indeed together all criteria, we obtain the official number of MM-like structures in Venus's magnetosheath. In Fig. 5 we show the daily occurrence rate of these structures over the whole VEX mission, with overplotted in red a 7-day running average. The average number of events per day is $\langle N \rangle = 21 \pm 21$.

Figures 6, 7 and 8 show the overall results of our analysis, for the whole data set, and for solar minimum and maximum conditions, respectively. Displayed are the residence time of VEX around Venus, the probability $\mathcal{P}$ to find MM-like structures in the $X - R$-plane and the average depth of $\Delta B/B$ in each grid cell.

The probability of MM-like structures for solar, minimum and maximum respectively for the cleaned data set, i.e. with the requirements $1 - 5$ from Sect. 2.2 applied. As mentioned above, there seem to be two regions in which this rate is greatly enhanced compared to the rest of Venus's surroundings: just behind the bow shock and around the ionopause. Similarly, Figs. 7 and 8 (right panels) show the average depth of the observed MM-like structures in each bin. As shown in Table 1 the average values for $\langle \Delta B/B \rangle$ are rather small for this data set, however the full distribution of $\Delta B/B$ is shown in Fig. 9.

First, we look at the depth of the MM-like structures. Fig. 9 shows the distribution of the depth $\Delta B/B$ of the MM-like structures, where the majority of the MM-like structures falls into the greyed-out category $0.05 \leq \Delta B/B \leq 0.15$, which are not taken into account in the analysis as per the selection criteria.

Both distributions are very similar percentage-wise, indicating that solar activity has little influence on the depth. However, one can discern a dichotomy in the percentages between solar minimum and maximum. The green bars, describing the ratio of the percentages of solar minimum and maximum ($\mathcal{G}$ = blue/red, multiplied by 10 for visibility) show that up until $\Delta B/B = 0.5$, there is a higher percentage for solar minimum, $\mathcal{G} > \infty$, and after that for solar maximum, $\mathcal{G} < \infty$. It was shown above that the location of the MM-like structures is different as well as the total amount of MM-like structures measured: 40987 and 59237, respectively (see Table 1). Especially, very deep events, $\Delta B/B \geq 0.75$, are ~ 5 times more abundant at solar maximum as compared to solar minimum, with 1973 and 357 events, respectively.
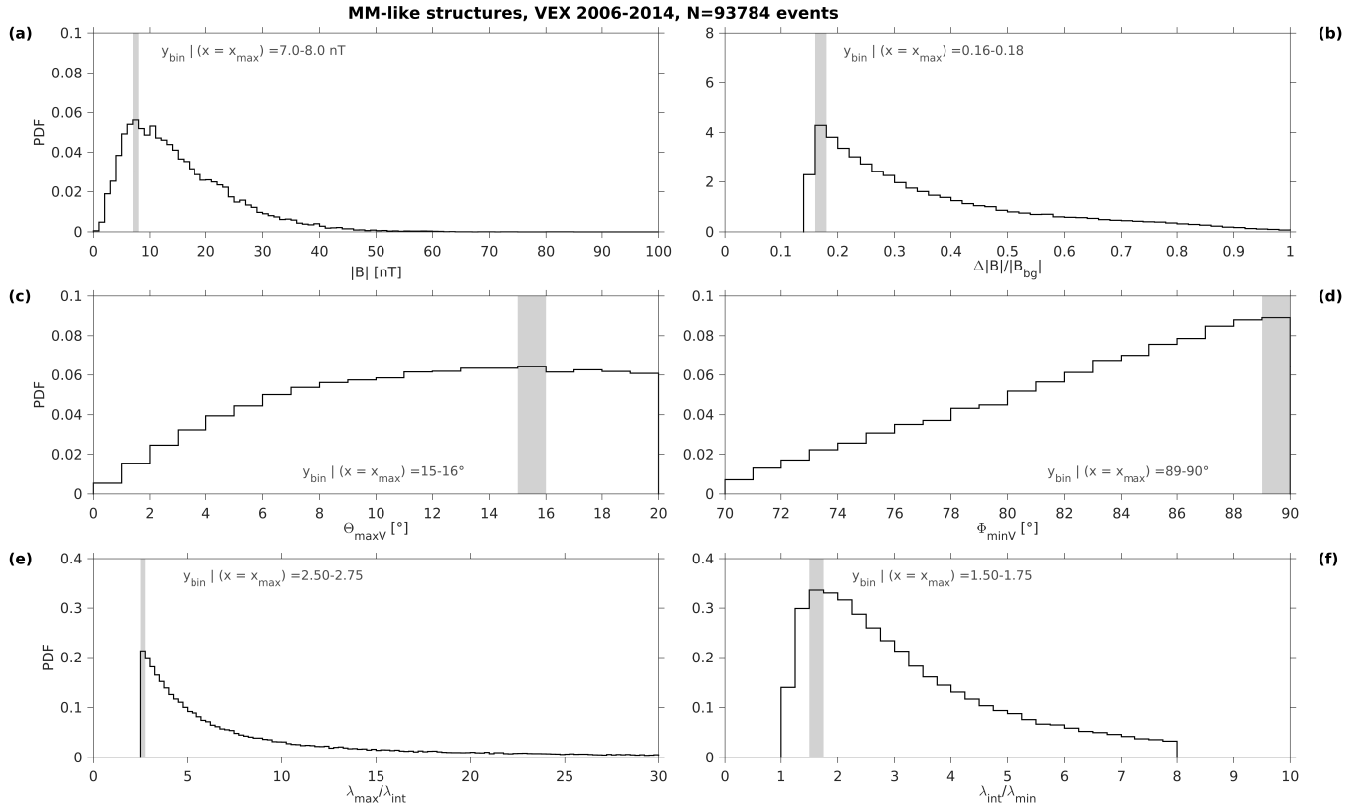
Figure 4. Probability Distribution Functions (PDFs) of selection criteria for MM-like structures in the VEX magnetometer data for the whole mission. (a): Total magnetic field intensity $|\mathbf{B}|$, in bins of 1 nT. (b) Magnetic field fluctuations $\Delta|\mathbf{B}|/B_{\mathrm{bg}}$, in bins of 0.02. (c) and (d): Angles between average magnetic field direction and maximum (minimum) variance direction Θ_{maxV} (Φ_{minV}), in bins of 1°. (e) and (f): Ratios of maximum to intermediate $\lambda_{\mathrm{max}}/\lambda_{\mathrm{int}}$ (intermediate to minimum, $\lambda_{\mathrm{int}}/\lambda_{\mathrm{min}}$) eigenvalues, in bins of 0.25. The position of the maximum of the PDF and its typical bin is marked by a grey zone. All bins are uniformly distributed.

3.2 Study of the observational dependence on physical parameters

It was shown above that the main differences of the probability of MM-like structures for solar minimum and maximum are: (1) the total number of events measured, and (2) the location within the magnetosheath where they were observed. As previously pointed out, no seasonal variations in the probability is expected. However, there can be other effects that can have an influence
225 on the probability of MM-like structures.

As the MM-like structures behind the BS are mainly generated by freshly created pick-up ions, re-energized by their crossing of the bow shock, it stands to reason that the solar EUV flux plays a role, as photo-ionization is the main source for these particles. Indeed, it was shown by Delva et al. (2015) that the higher number of observed proton cyclotron waves for solar maximum, as compared to minimum, was caused by the higher EUV flux, supplying a greater number of newborn protons
230 from Venus's exosphere.
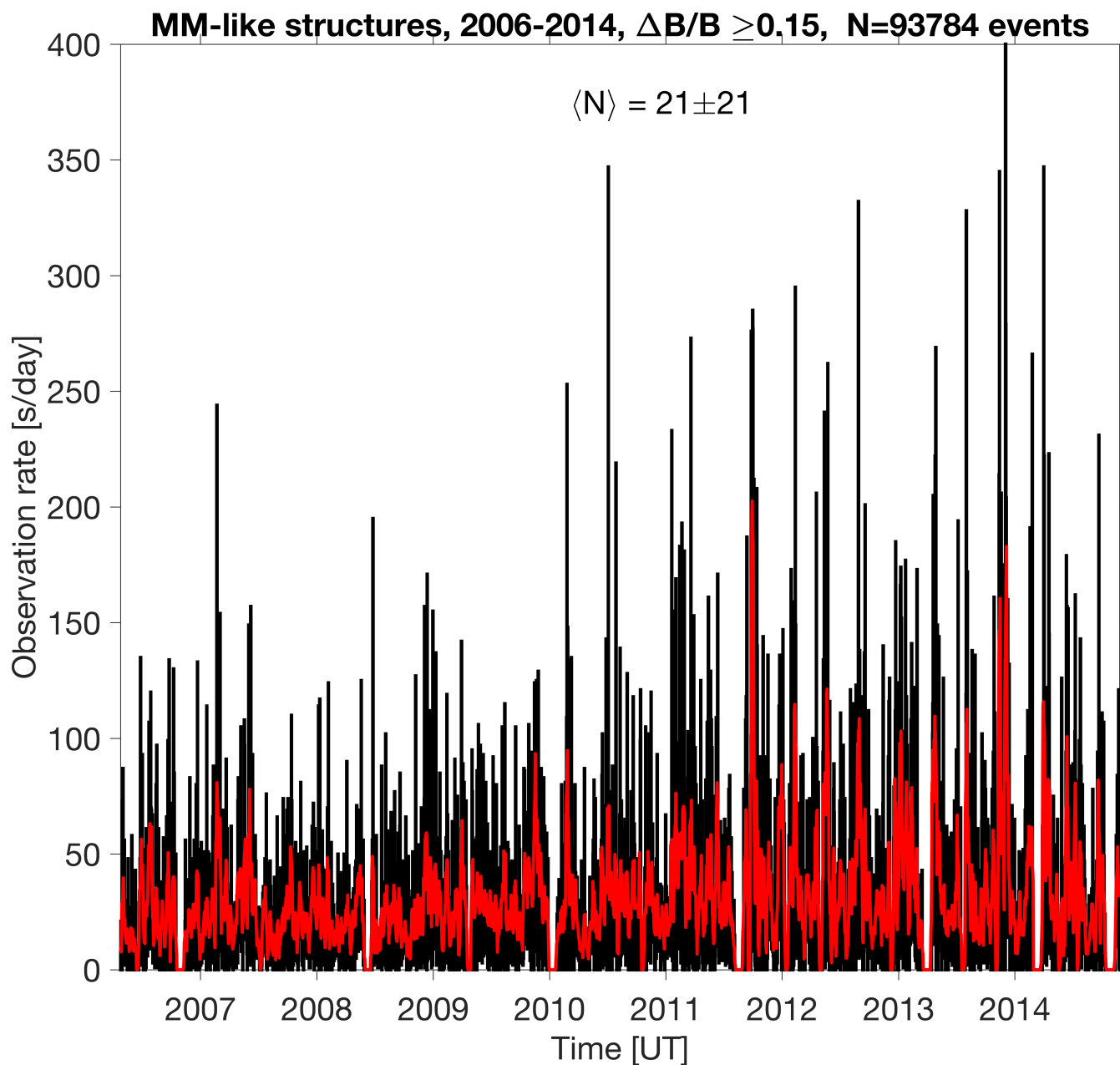
Figure 5. Daily observation rate of MM-like structures as observed by the VEX magnetometer for the whole mission, using the selection criteria mentioned in Sect. 2.2. The red line corresponds to the running mean of the black curve over 7 days. $\langle N \rangle$ is the median of the signal in black, with its corresponding standard deviation.
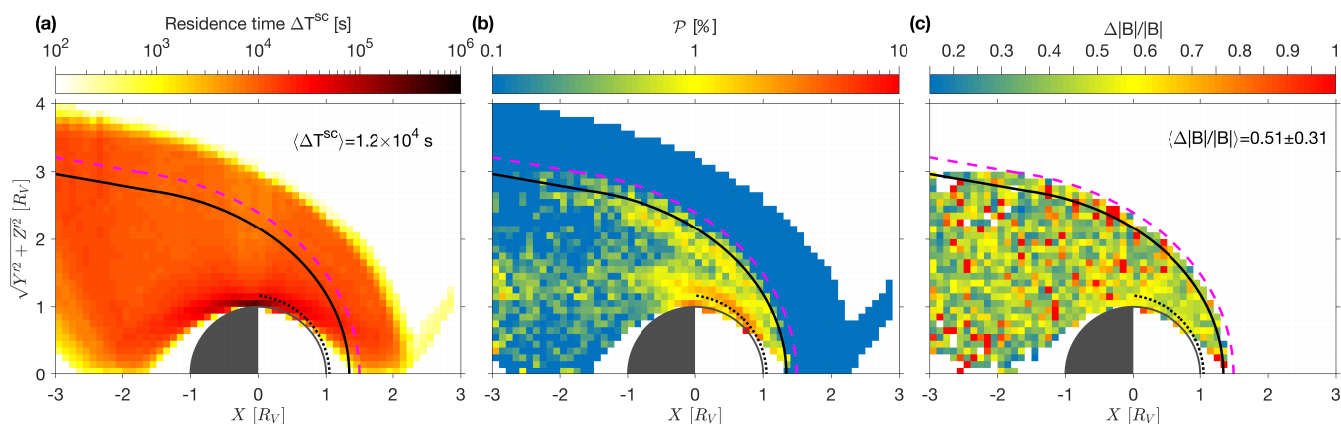
Figure 6. Full data set: (left) The total residence time of Venus Express in the $X - R$-plane. The thick black line is the bow shock location as determined by Zhang et al. (2008) for solar minimum. The dotted line is the magnetopause/ionopause location.(middle) The probability of MM-like structures in the $X - R$-plane. There are two clear regions of increased $\mathcal{P}$, just behind the bow shock and close to the magnetopause/ionopause. (right) The average depth of the mirror modes in each grid cell, limited by $\Delta B/B \geq 0.15$.
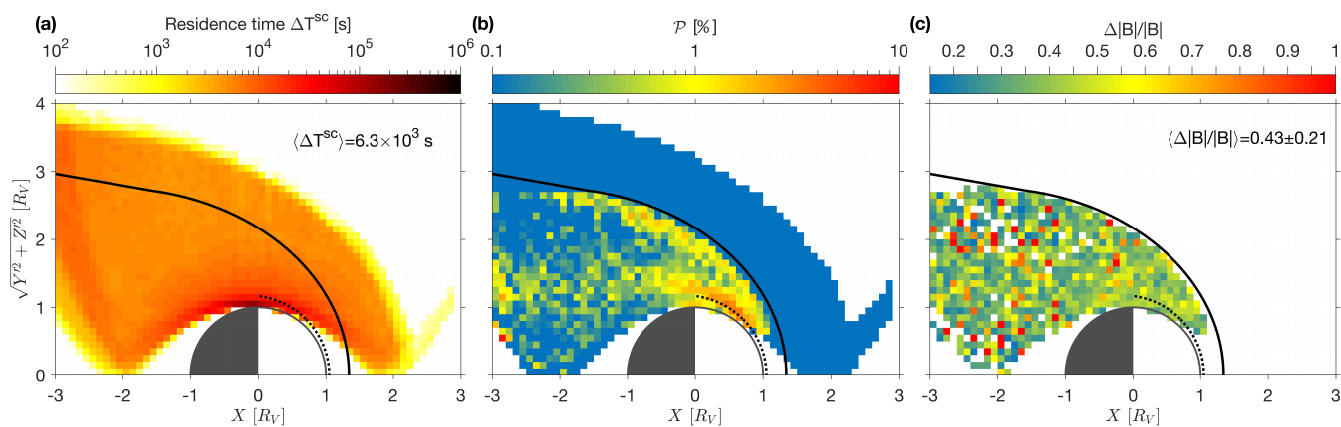
Figure 7. Solar Minimum: same format as Fig. 6.
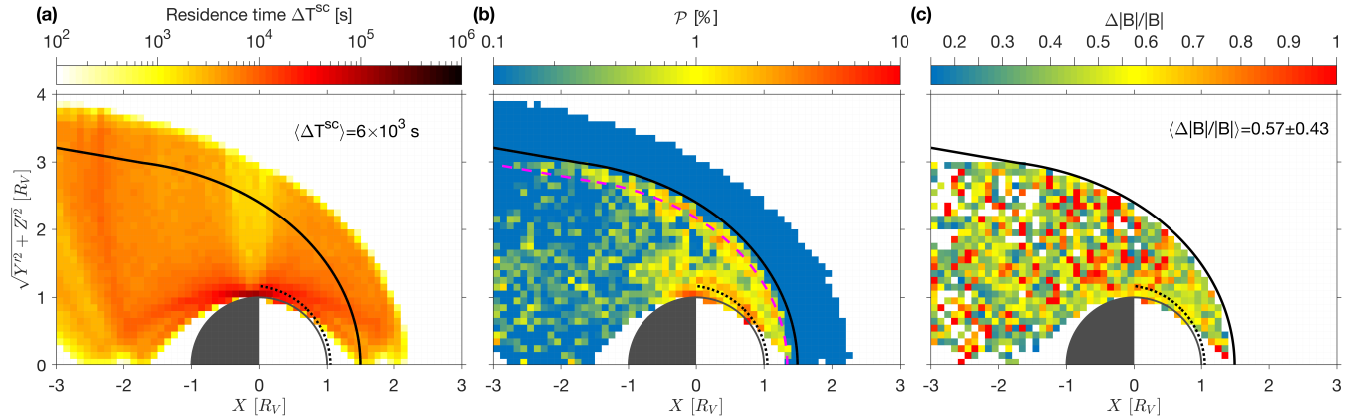
Figure 8. Solar Maximum: same format as Fig. 6.

The split between solar minimum and maximum based on sunspots is rather arbitrary and a more sophisticated method can be used to study the influence of solar activity, through the daily F10.7 flux. As can be seen in Fig. 1, however, the divide assumed in this paper splits the periods well with $\#\text{sunspots} \lessgtr 50$, or $F10.7 \lessgtr 100$ SFU. Every event is assigned its corresponding daily averaged F10.7 value. Figure 10 shows the histogram of the daily F10.7 value over the whole mission in percentages of the total days, as well as that for the events in percentages of the total number of events. It is clear that both histograms show a similar trend, with only slight difference of a few percentage-points. The yellow bars show the ratio of percentage event flux over percentage daily flux $\mathcal{Y}$ (yellow = red/blue, multiplied by 10 for visibility). The dotted vertical line shows the division between solar minimum and maximum. The average ratio for solar minimum is $\overline{\mathcal{Y}} \approx 0.9$, whereas for solar maximum $\overline{\mathcal{Y}} \approx 1.5$ (limiting to values $F10.7 \leq 200$ SFU). This means that there is a slight influence of the F10.7 flux onto the creation of MM-like structures, such that at solar maximum the structures are prone to exist for higher flux, whereas for solar minimum both the daily and event fluxes are basically equal.

4 Discussion

We have studied the probability of mirror mode like structures in Venus's magnetosheath over the whole Venus Express mission, with the strict constraints as presented in Paper 1. The outcome can be compared to the previous study on MM-like structures by Volwerk et al. (2016) and a recent study of the plasma properties around Venus by Rojas Mata et al. (2022).

The whole Venus Express mission extended over most of a solar cycle, where both solar minimum and maximum are sampled well, as shown in Fig. 1 and in Table 1 for $\Delta T_{\text{tot}}^{\text{sc}}$. There are two main differences between these two periods with respect to the MM-like structures: (1) The total number of events and probability are larger for solar maximum; (2) the location of observations are different with the MM-like events found deeper in the magnetosheath for solar maximum.

There is a slight difference in the distribution of the depth, $\Delta B/B$, of the MM-like structures for solar minimum and maximum (see Fig. 9). For solar minimum there are more weaker MM-like structures, whereas for solar maximum there are
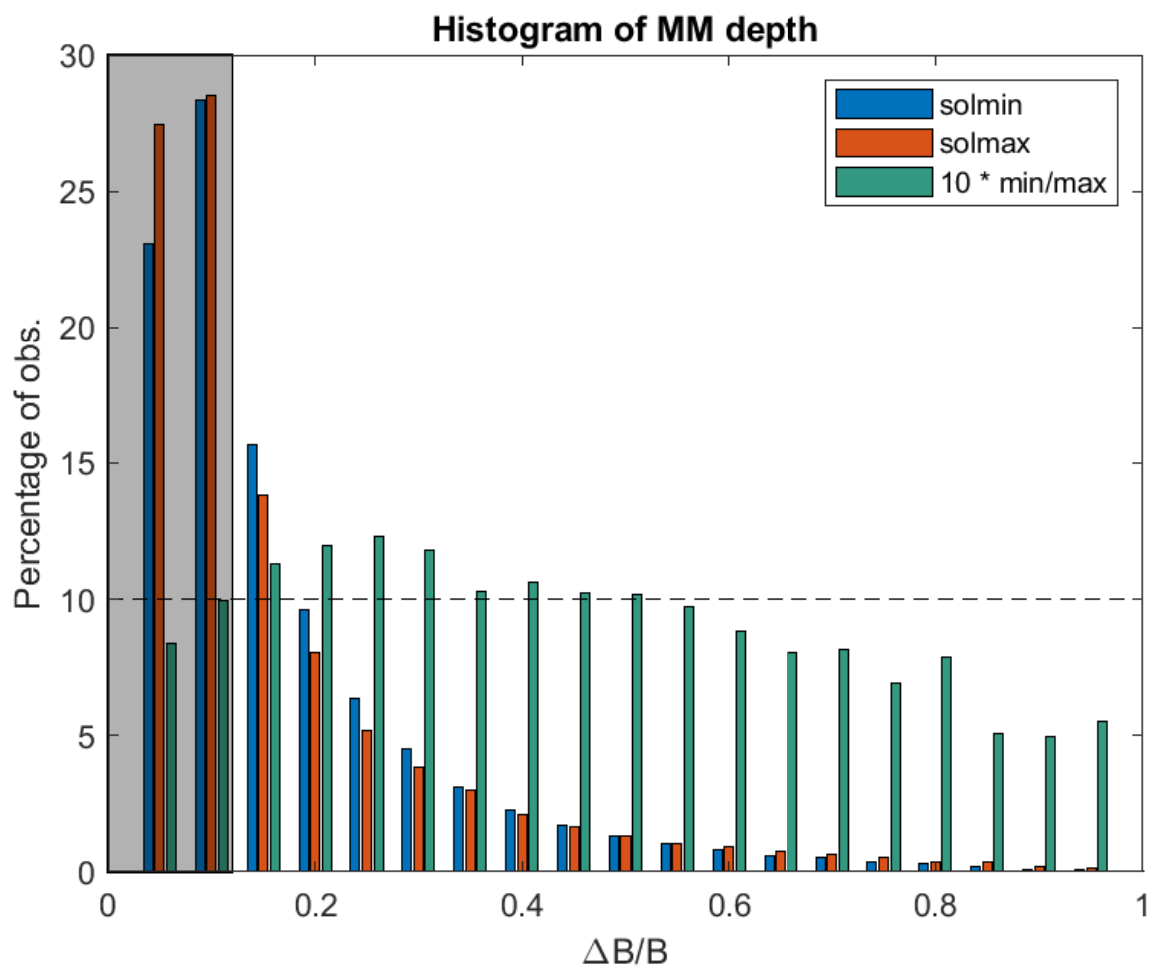
Figure 9. Histograms of the distribution of the depth $\Delta B/B$ of the MM-like structures for solar minimum (blue) and maximum (red) and the ratio between the two (green = blue/red, multiplied by 10 for visibility). The grey shaded region shows the structures with $\Delta B/B < 0.15$ that are not taken into account in the analysis in this paper.
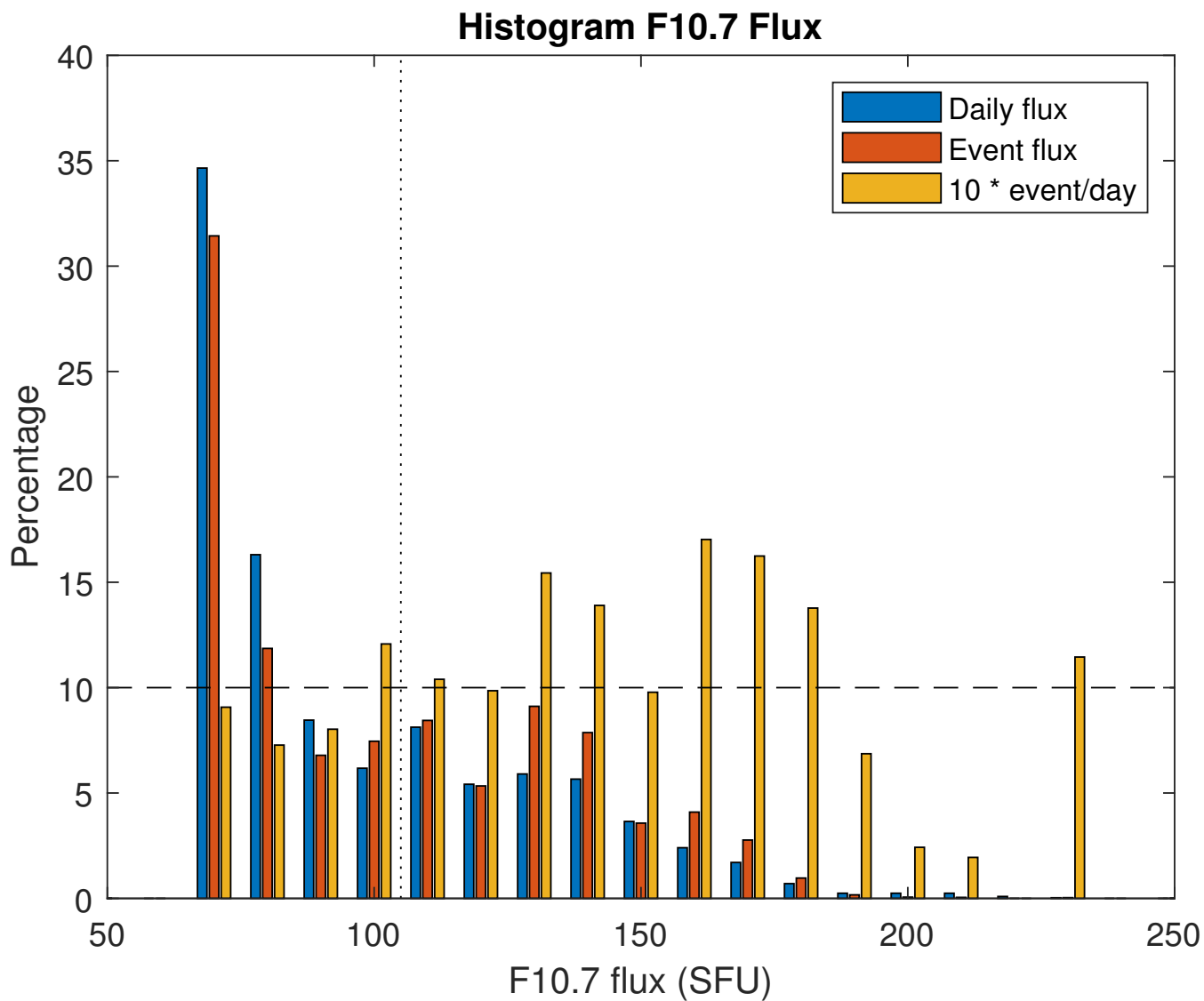
Figure 10. Histograms of the F10.7 flux. Combined are the distribution of the percentages of daily flux (blue) and of the flux for each event specifically (red). The yellow bars show the ratio of the two fluxes (yellow = red/blue, multiplied by 10 for visibility).

more stronger structures. Similarly, there is a slight dependence of the observation of MM-like structures with respect to the F10.7 flux. The event flux is higher than the daily average flux during solar maximum, whereas for solar minimum they are almost equal.

This means that only the generation of MM-like structures is strongly dependent on solar activity: more activity leads to more ionization, which in its turn leads to more ion pick-up and crossings of the instability threshold, Eq. (1). But there seems to be no evolutionary development of the MM-like structures with respect to their depth, not through increased solar activity. There could be a temporal development while they are transported by the plasma flow, which will be discussed further below in Sect. 4.1.

Looking at the locations of the maxima of the probabilities $\mathcal{P}$ in Figs. 7 and 8 one finds that the MM-like structures identified just behind the bow shock are deeper inside the magnetosheath for solar maximum than for solar minimum. In Fig. 8, middle panel, the bow shock location for solar minimum has also been indicated by a dashed magenta line. This panel shows that the maximum probability is at the location of this magenta line. It is unclear whether this is just by chance or if this location has a physical meaning.

4.1 Comparison with Volwerk et al.

Mirror modes in Venus's magnetosheath were first discovered by Volwerk et al. (2008a, b) and a comparison between solar minimum and solar maximum was presented in Volwerk et al. (2016). These studies, however, were based on only one Venus-year (223 Earth days) of data for each solar activity level. Nevertheless, some of the results from those papers are in agreement with the results presented above for the full 2006-2014 VEX dataset.

Figure 11 shows the occurrence rate of the MM-like structures on a coarser grid of $0.25 \times 0.25\,R_V$. Note that the definition of the occurrence rate in the papers by Volwerk et al. is different than in our present study. Volwerk et al. gathered together closely spaced intervals to obtain MM events, separated by at least 30 s, whereas in our study the total number of seconds for which the MM conditions are fulfilled is used. We expect that these different ways of assessing MM-like structures are still comparable on average. It is clear that these plots shows less structure than the middle panels of Figs. 7 and 8 because of the lesser amount of data and the coarser grid. We will compare a few of their conclusions with the results in the present study. Volwerk et al. (2016) state that:

1. The number of MM-like structures at solar maximum is higher than at solar minimum by $\sim 14\%$;

2. The probability for both solar conditions is the same for solar minimum and maximum;

3. The distribution of $\Delta B/B$ is exponential with approximately the same coefficient for both solar conditions;

4. For solar minimum the general trend for MM-like structures is to decay; for solar maximum MM-like structures first grow and then decay, between the bow shock and the terminator;

Point (1) is in general agreement with what is shown in Table 1, albeit that the increase for solar maximum is $\sim 45\%$, even though the total residence time for solar maximum was $\sim 10\%$ less. This again has influence on point (2), regarding
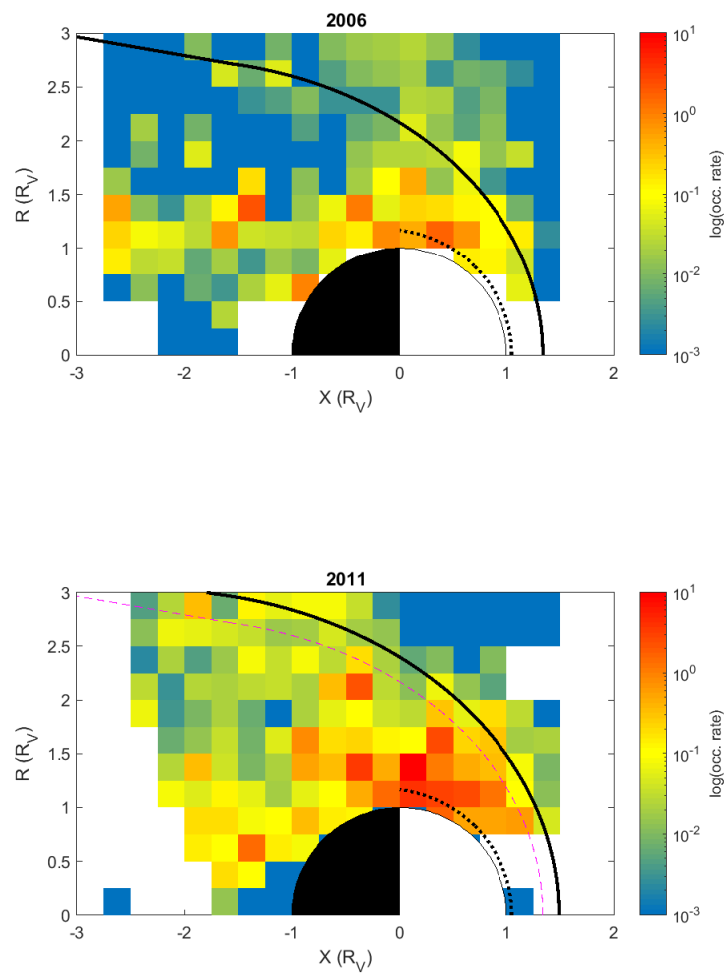
Figure 11. The occurrence rate for one Venus year at solar minimum (2006) and maximum (2011) reproduced from Volwerk et al. (2016) on a grid of $0.25 \times 0.25\,R_V$. This shows less structure than the middle panels of Figs. 7 and 8.

the probability. In our present study we find that in total the probabilities of detection of MM-like structures are ~ 0.05 and ~ 0.08 for solar minimum and maximum (Table 1), respectively, i.e. a multiplication factor $\times 1.6$, between solar minimum and solar maximum conditions. This shows that considering a larger statistical data set for this kind of study greatly influences the statistical results.

Fig. 9 shows the distribution of $\Delta B/B$, which seems to indicate an exponential drop-off as in point (3). Volwerk et al. (2016) found two different e-folding lengths, b, through a fit by:

$$y = a * \exp\{b \times \Delta B/B\}, \tag{7}$$

describing the distribution for "weak" ($\Delta B/B < 0.6$) and "strong" ($\Delta B/B > 0.4$) MM-like structures[4], with $b \approx -3.4$ and $b \approx -2.5$ respectively, for solar minimum and maximum conditions. In our present study the data seem to show also an exponential decay, however with three slopes (see Fig. 12): $b \approx -9.9$, $b \approx -5.4$, and $b \approx -10.5$. This significantly differs from earlier observations.

Looking at the distribution of the occurrence rate, and fitting the median and upper/lower-quartiles of $\Delta B/B$ taken in $0.25\,R_{\mathrm{V}}$-bins, Volwerk et al. (2016) found that for solar minimum there was a decrease of these numbers from the bow shock away, whereas for solar maximum these values were first increasing and then decreasing.

In Fig. 13, we first calculate the distance of any event on the map to the bow shock along the X_{VSO} line, with $R_{\mathrm{VSO}} = $ constant. $\Delta B/B$ is plotted for three R_{vso}-intervals. The vertical red lines show the average location of the terminator with respect to the shock. In the panels the mean (red) and standard deviation (green) are overplotted. There is an increase in the depth of the structures towards the terminator and slightly behin, although in the bottom panels for $1.0 \leq R \leq 1.2$ this is not quite visible in the mean and standard deviation.

This is different from Volwerk et al. (2016), where it was stated that the MM-like structures decay away from the BS at solar minimum and first grow and then decay at solar maximum. At better statistics, this is not the case, there is a drop in maximum $\Delta B/B$ from the BS inward, i.e. from 0 to $\sim 0.25\,R_{\mathrm{V}}$, for both situations.

4.2 Comparison with Rojas Mata et al.

Lately, Rojas Mata et al. (2022) have studied the Ion Mass Analyzer (IMA) proton data of the ASPERA-4 instrument, showing the proton temperature anisotropies during the whole VEX mission, divided up into solar minimum and maximum, similar as in our present study. In Fig. 14 the temperature ratio $\mathcal{T} = \mathrm{median}(T_\perp/T_\parallel)$ for each grid cell is shown on a smaller grid ($0.1 \times 0.1\,R_{\mathrm{V}}$) than in the original paper The overall trends are similar for both grid resolutions except a few random "outlier-looking" bins. It was found that the highest temperature asymmetry, $\mathcal{T}$, lies deeper inside the magnetosheath for solar maximum. Indeed, the same conclusion can be made from Fig. 14, where, like in the occurrence rate in Fig. 8, we have plotted the solar minimum location of the bow shock as a magenta dashed line. Interestingly, this line seems to lie well along the boundary of the maximum $\mathcal{T}$.

---

[4]The depth of the MM-like structures has been adjusted to agree with the definition in this current paper.
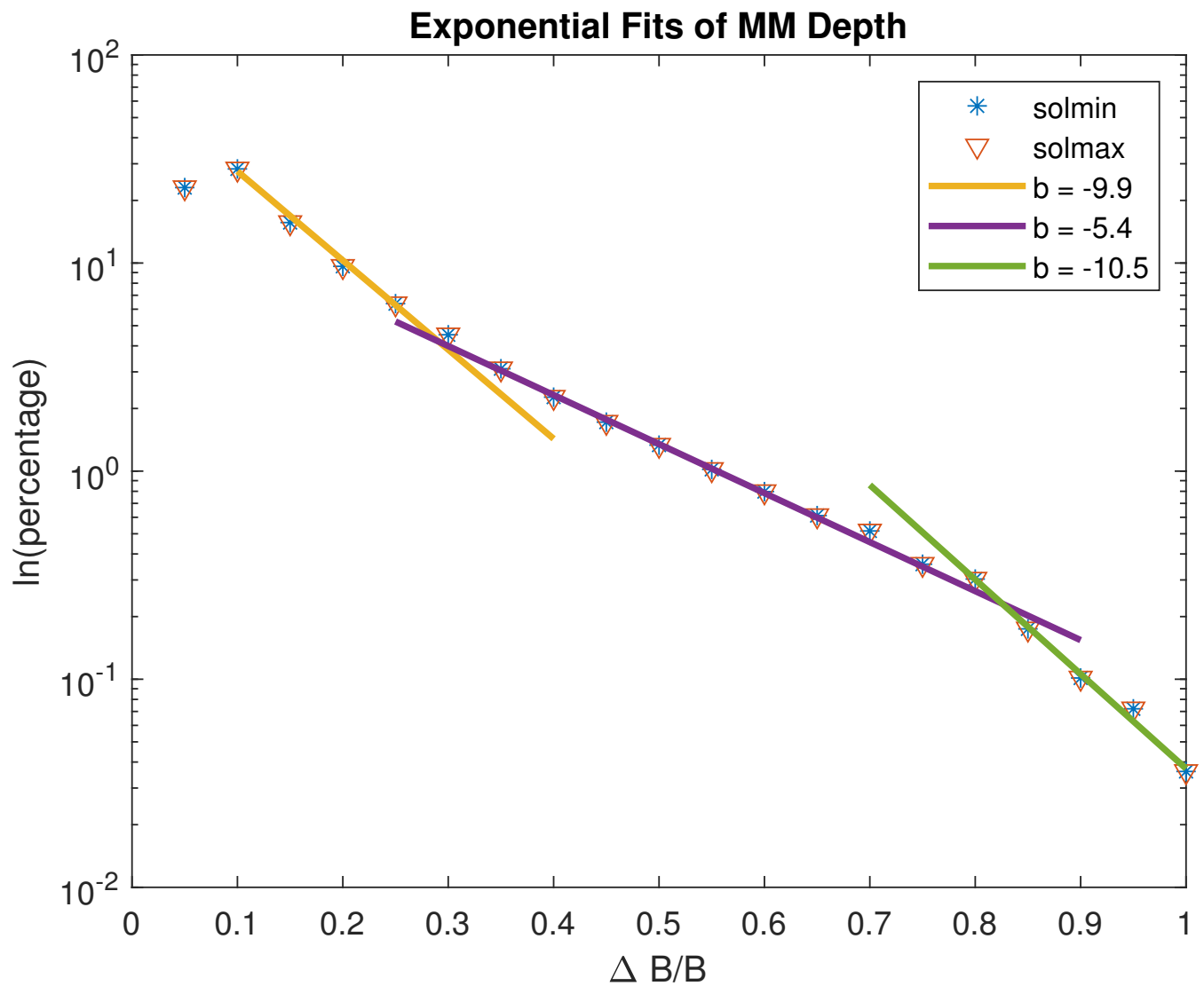
Figure 12. Exponential fits to the depth distribution of the MM-like structures for solar minimum and maximum. Three different regions can be identified and the slopes b for the fits $y = a * \exp\{b \times \Delta B/B\}$ can be found in the legend.
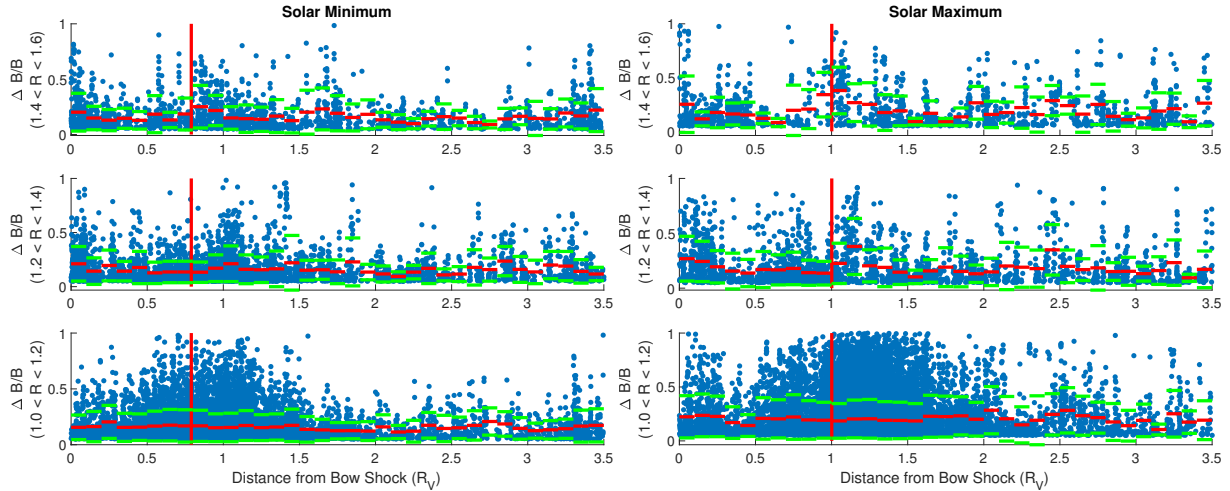
Figure 13. $\Delta B/B$ as a function of distance from the bow shock for three intervals $1.0 \leq R \leq 1.2$, $1.2 \leq R \leq 1.4$ and $1.4 \leq R \leq 1.6$. The red vertical line shows the distance of the terminator to the bow shock in the $1.0 \leq R \leq 1.5$ bin.

315   It should be noticed that there is a bias in the comparison between the ASPERA-4 data, with 192 s resolution and the magnetometer resolution of 1 s. The ion data will show larger local variations as with the orbital velocity of VEX of ~ 8 km/s this results in a size of ~ 1500 km or $\sim 0.25\,R_{\mathrm{V}}$ (the tentative reason to have this grid cell size in Rojas Mata et al. (2022)), although this does not take into account the (much) faster plasma flow in the magnetosheath. However, the averaging done in the grid cells might reduce this effect slightly in the statistics.

320   Comparing the $\mathcal{P}$ distributions in the middle panels of Figs. 7 and 8 with $\mathcal{T}$ in Fig. 14 one notices that, as said above, there are two regions of maximum $\mathcal{P}$, whereas the maximum of $\mathcal{T}$ seems to fall in-between these two regions. The effect is most clearly visible for solar maximum conditions. This shows that the presence of MM-like structures locally reduces the (median) temperature ratio $\mathcal{T}$ in the magnetosheath, an indication that the instability transfers its energy from the ions to the waves.

Figure 15 shows the percentage of scans in each $0.1 \times 0.1\,R_{\mathrm{V}}$ cell, for which the instability criterion $\mathrm{MMI} < 0$ (Eq. 1) is
325   fulfilled. Note the large difference between the two solar conditions: although the criterion is fulfilled much more frequently at solar minimum than at solar maximum, there are fewer MM-like structures on average as shown in Figs. 7 and 8. This points at an extra necessity for MM-like structures to start to develop, apart from the instability criterion of Eq. (1)

5   Conclusions

We have studied the magnetic field data for the whole Venus Express mission and searched for mirror modes in the magne-
330   tosheath. The VEX mission has been split-up into two parts, corresponding to solar minimum and solar maximum, for which one of the main differences is that the bow shock for solar maximum is further out at $\sim 1.49\,R_{\mathrm{V}}$ as compared to $\sim 1.34\,R_{\mathrm{V}}$ for solar minimum at the subsolar point.
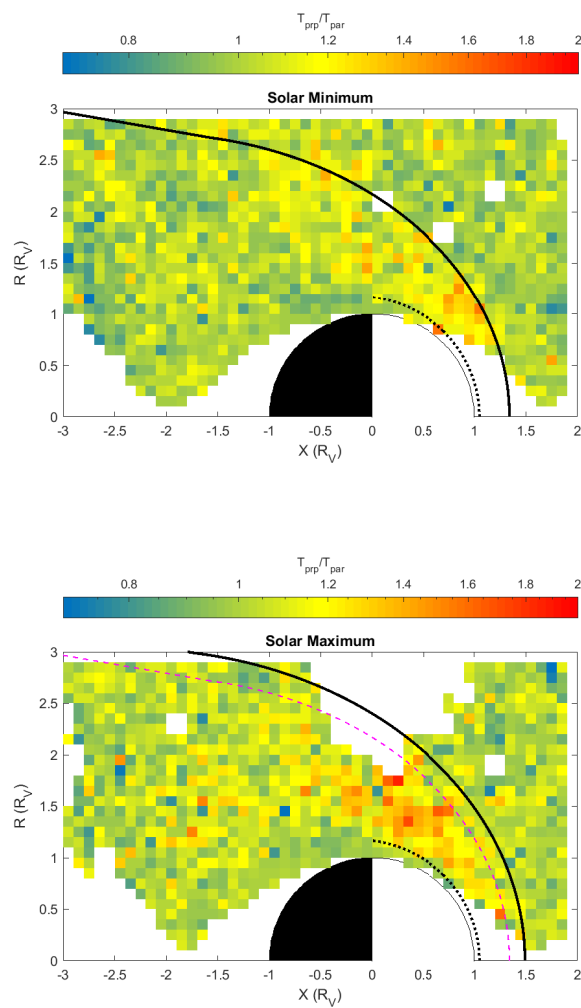
Figure 14. The temperature ratio $\mathcal{T} = \mathrm{median}(T_\perp/T_\parallel)$ for each grid box around Venus for solar minimum (top) and maximum (bottom). The data have been re-evaluated on a $0.1 \times 0.1\,R_V$ grid from the study by Rojas Mata et al. (2022).
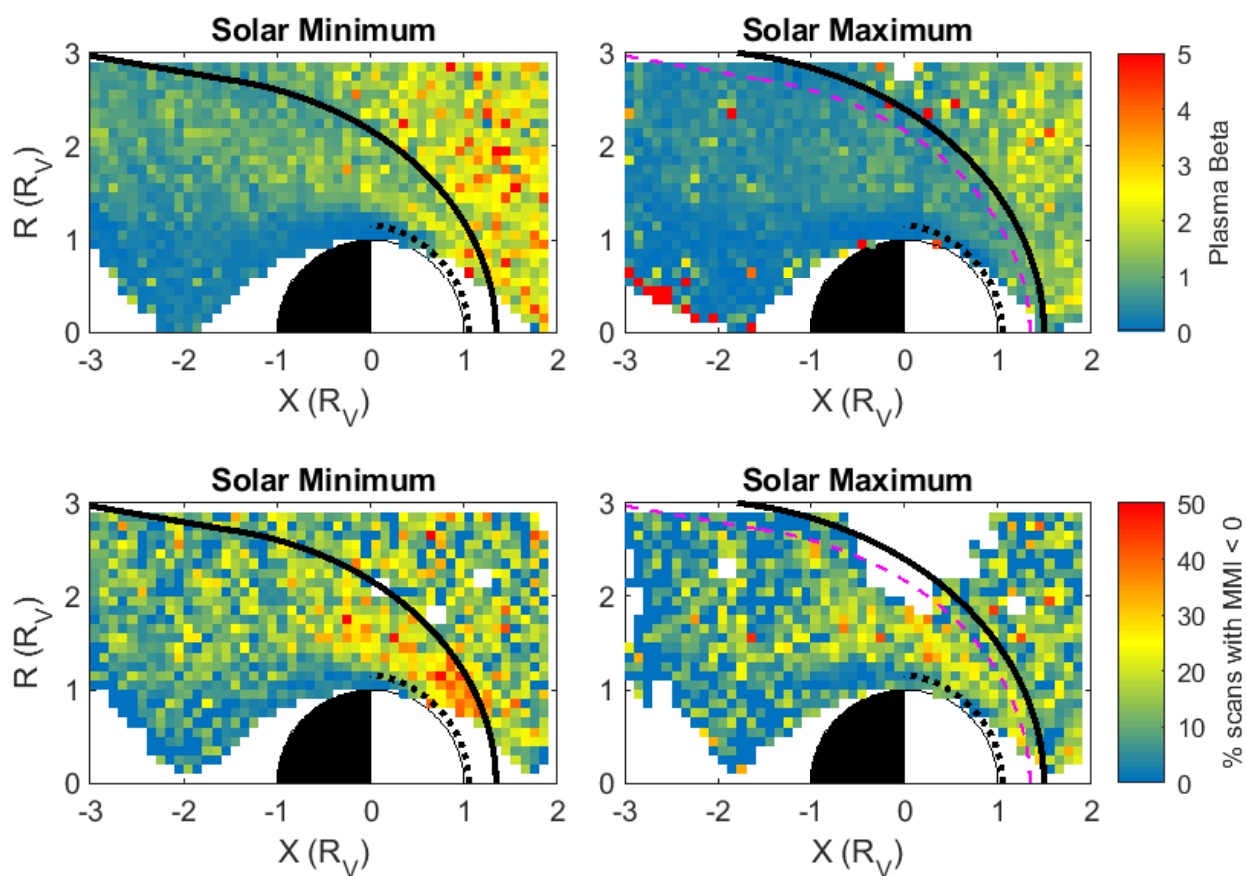
Figure 15. Top: The mean plasma-β in Venus's environment. Bottom: The percentage of scans in each box for which the instability criterion, Eq. (1), $\mathrm{MMI} < 0$. The data have been re-evaluated on a $0.1 \times 0.1\,R_{\mathrm{V}}$ grid from the study by Rojas Mata et al. (2022).

The total probability $\mathcal{P}$ for solar maximum lies higher than for solar minimum even when normalising to the total observation time for each condition. The regions where the MM-like structures are observed are behind the BS and near the

335   magnetopause/ionopause. But behind the BS, the probability $\mathcal{P}$ peaks further inside the magnetosheath for solar maximum. Comparison with the proton data shows that $\mathcal{P}$ peaks where the temperature asymmetry, $\mathcal{T}$, is reduced, indicating that energy has been transferred from the ions to the waves.

The total probablity $\mathcal{P}$ is lower for solar miminum than for solar maximum (Table 1), but Fig. 15 shows that the percentage of scans with $MMI < 0$ is larger for solar minimum. Again this raises the question whether there is more to the creation of

340   MM-like structures than just the instability criterion. The major difference in the two periods is the plasma-β, shown in Fig. 15 (top panels) which is much higher for solar minimum (as also observed by Wilson et al., 2018, in the solar wind at 1 au). This extra thermal energy does not seem to drive more or even deeper MM-like structures as shown in Fig. 9. Quite possibly, there is a competing effect: Rojas Mata et al. (2022) show that there is a higher compression of the IMF during solar maximum in the dayside magnetosheath. This would decrease the plasma-β, but through the first adiabatic variant mechanism it could

345   increase the perpendicular temperature and thereby increase the β and the anisotropy. Indeed, in the magnetosheath behind the quasi-perpendicular bow shock an inverse correlation was found with variations between high-β - low temperature anisotropy and low-β - high temperature anisotropy (Anderson and Fuselier, 1993, 1994; Anderson et al., 1994; Fuselier et al., 1994).

The distribution of the depth of the MM-like structures does not seem to be strongly dependent on solar conditions. The distribution seems to be exponential, but closer inspection shows a combination of three different exponential slopes, with no

350   difference between solar minimum and maximum. Also, solar irradiance, with proxy the F10.7 flux, does not seem to influence the number of MM-like structures.

There remain some open questions after this study. Why are there *large* regions where the temperature asymmetry, $\mathcal{T}$, is enhanced and the MM probability, $\mathcal{P}$, reduced? What are the extra conditions for MM-like structures to start to grow in the magnetosheath plasma? How do quasi-perpendicular and quasi-parallel shock conditions impact the distribution and frequency

355   of the observed structures? What is the dependence on solar wind IMF conditions?Also, the location of the solar minimum bow shock seems to take a special place, as during solar maximum it is the boundary where the probability, $\mathcal{P}$, strongly increases.

Data availability. The Venus Express magnetometer and IMA data are available through ESA's Planetary Science Archive, https://archives. esac.esa.int/psa. The F10.7 daily flux was obtained from LISIRD, https://lasp.colorado.edu/lisird/data/noaa_radio_flux.

Author contributions. MV and CSW instigated the investigation. DM analysed the magnetometer data. MD calibrated the magnetometer

360   data. SRM analysed the ASPERA-4 ion data. GSW, YF, CM, JH. DRC, and CB helped interpreting the results of the data analysis and in writing the paper.

Competing interests. There are no competing interests.

Acknowledgements. The work of CSW and DM is sponsored by the Austrian Science Fund (FWF) under project number P32035-N36. SRM was funded by the Swedish National Space Agency under contract 145/19 and 79/19. The authors thank ISSI and the ISSI international team
365 517 "Towards a Unifying Model for Magnetic Depressions in Space Plasmas" for facilitating research between team members.

References

Anderson, B. J. and Fuselier, S. A.: Magnetic pulsations from 0.1 to 4.0 Hz and associated plasma properties in the Earth's magne-tosheath and plasma depletion layer, J. Geophys. Res., 98, 1461 – 1480, https://doi.org/10.1029/92JA02197, 1993.

Anderson, B. J. and Fuselier, S. A.: Erratum: "Magnetic pulsations from 0.1 to 4.0 Hz and associated plasma properties in the Earth's subsolar magnetosheath and plasma depletion layer" [J. Geophys. Res. 98, 1461-1479 (1993)], J. Geophys. Res., 99, 6149 – 6150, https://doi.org/10.1029/93JA03041, 1994.

Anderson, B. J., Fuselier, S. A., Gary, S. P., and Denton, R. E.: Magnetic spectral signatures in the Earth's magnetosheath and plasma depletion layer, J. Geophys. Res., 99, 5877 – 5892, https://doi.org/10.1029/93JA02827, 1994.

Bader, A., Stenberg Wieser, G., André, M., Wieser, M., Futaana, Y., Persson, M., Nilsson, H., and Zhang, T. L.: Proton Temperature Anisotropies in the Plasma Environment of Venus, J. Geophys. Res., 124, 3312 – 3330, https://doi.org/10.1029/2019JA026619, 2019.

Barabash, S., Sauvaud, J.-A., Gunell, H., Andersson, H., Grigoriev, A., Brinkfeldt, K., Holmström, M., Lundin, R., Yamauchi, M., Asamura, K., Baumjohann, W., Zhang, T., Coates, A., Linder, D., Kataria, D., Curtis, C., Hsieh, K., Sandel, B., Fedorov, A., Mazelle, C., Thocaven, J.-J., Grande, M., Koskinen, H. E., Kallio, E., Säles, T., Riihela, P., Kozyra, J., Krupp, N., Woch, J., Luhmann, J., McKenna-Lawlor, S., Orsini, S., Cerulli-Irelli, R., Mura, M., Milillo, M., Maggi, M., Roelof, E., Brandt, P., Russell, C., Szego, K., Winningham, J., Frahm, R., Scherrer, J., Sharber, J., Wurz, P., and Bochsler, P.: The analyser of space plasmas and energetic atoms (ASPERA-4) for the Venus Express mission, Planet. Space Sci., 55, 1772 – 1792, https://doi.org/10.1016/j.pss.2007.01.014, 2007.

Baumjohann, W., Treumann, R. A., Georgescu, E., Haerendel, G., Fornaçon, K.-H., and Auster, U.: Waveform and packet structure of lion roars, Ann. Geophys., 17, 1528 – 1534, 1999.

Bavassano Cattaneo, M. B., Basile, C., Moreno, G., and Richardson, J. D.: Evolution of mirror structures in the magnetosheath of Saturn from the bow shock to the magnetopause, J. Geophys. Res., 103, 11 961 – 11 972, 1998.

Bertucci, C., Mazelle, C., Crider, D. H., Mitchell, D. L., Sauer, K., Acuna, M., Connerney, J. E. P., Lin, R. P., Ness, N. F., and Winterhalter, D.: MGS MAG/ER observations at the magnetic pileup boundary of Mars: draping enhancement and low frequency waves, Adv. Space Res., 33, 1938 – 1944, https://doi.org/10.1016/j.asr.2003.04.054, 2004.

Bohm, D., Burhop, E. H. S., and Massey, H. S. W.: The use of probes for plasma exploration in strong magnetic fields, in: The characteristics of electrical discharges in magnetic fields, edited by Guthrie, A. and Wakerling, R. K., pp. 13 – 76, McGraw-Hill, New York, 1949.

Delva, M., Zhang, T. L., Volwerk, M., Vörös, Z., and Pope, S. A.: Proton cyclotron waves in the solar wind at Venus, Geophys. Res. Lett., 113, E00B06, 2008.

Delva, M., Volwerk, M., Mazelle, C., Chauffray, J. Y., Bertaux, J. L., and Zhang, T. L.: Hydrogen in the extended Venus exosphere, Geophys. Res. Lett., 36, L01203, https://doi.org/10.1029/2008GL036164, 2009.

Delva, M., Mazelle, C., Bertucci, C., Volwerk, M., Vörös, Z., and Zhang, T. L.: Proton cyclotron wave generation mechanisms upstream of Venus, J. Geophys. Res., 116, A02318, 2011.

Delva, M., Bertucci, C., Volwerk, M., Lundin, R., Mazelle, C., and Romanelli, N.: Upstream proton cyclotron waves at Venus near solar maximum, J. Geophys. Res., 120, 344 – 354, https://doi.org/10.1002/2014JA020318, 2015.

Erdös, G. and Balogh, A.: Statistical properties of mirror mode structures observed by Ulysses in the magnetosheath of Jupiter, J. Geophys. Res., 101, 1 – 12, https://doi.org/10.1029/95JA02207, 1996.

Espley, J. R., Cloutier, P. A., Brain, D. A., Crider, D. H., and Acuna, M. H.: Observations of low-frequency magnetic oscillations in the Martian magnetosheath, magnetic pileup region, and tail, J. Geophys. Res., 109, A07213, https://doi.org/10.1029/2003JA010193, 2004.

Fuselier, S. A., Anderson, B. J., Gary, S. P., and Denton, R. E.: Inverse correlations between the ion temperature anisotropy and plasma beta in the Earth's quasi-parallel magnetosheath, J. Geophys. Res., 99, 14 931 – 14 936, https://doi.org/10.1029/94JA00865, 1994.

405 Gary, S. P.: The Mirror and Ion Cyclotron Anisotropy Instabilities, J. Geophys. Res., 97, 8519 – 8529, https://doi.org/10.1029/92JA00299, 1992.

Gary, S. P., Fuselier, S. A., and Anderson, B. J.: Ion anisotropy instabilities in the magnetosheath, J. Geophys. Res., 98, 1481–1488, https://doi.org/10.1029/92JA01844, 1993.

Glassmeier, K. H., Motschmann, U., Mazalle, C., Neubauer, F. M., Sauer, K., Fuselier, S. A., and Acuna, M. H.: Mirror modes and fast
410 magnetoaucoustic waves near the magnetic pileup boundary of comet P/Halley, J. Geophys. Res., 98, 20 955–20 964, 1993.

Hasegawa, A.: Drift mirror instability in the magnetosphere, Phys. Fluids, 12, 2642–2650, 1969.

Hasegawa, A. and Tsurutani, B. T.: Mirror mode expansion in planetary magnetosheaths: Bohm-like diffusion, Phys. Rev. Lett., 107, 245005, https://doi.org/10.1103/PhysRevLett.107.245005, 2011.

Joy, S. P., Kivelson, M. G., Walker, R. J., Khurana, K. K., and Russell, C. T.: Mirror mode structures in the Jovian magnetosheath, J. Geophys.
415 Res., 111, A12212, https://doi.org/10.1029/2006JA011985, 2006.

Lucek, E. A., Dunlop, M. W., Balogh, A., Cargill, P., Baumjohann, W., Georgescu, E., Haerendel, G., and Fornacon, K.-H.: Identification of magnetosheath mirror modes in Equator-S magnetic field data, Ann. Geophys., 17, 1560 – 1573, 1999a.

Lucek, E. A., Dunlop, M. W., Balogh, A., Cargill, P., Baumjohann, W., Georgescu, E., Haerendel, G., and Fornacon, K.-H.: Mirror mode structures observed in the dawn-side magnetosheath by Equator-S, Geophys. Res. Lett., 26, 2159 – 2162, 1999b.

420 Mazelle, C., Belmont, G., Glassmeier, K. H., LeQuéau, D., and Réme, H.: Ultralow frequency waves at the magnetic pile-up boundary of comet P/Halley, Adv. Space Res., 11, 73 – 77, 1991.

McComas, D. J., Angold, N., Elliott, H. A., Livadiotis, G., Schwadron, N. A., Skoug, R. M., and Smith, C. W.: Weakest solar wind of the space age and the current "mini" solar maximum, Astrophys. J., 779, 2, https://doi.org/10.1088/0004-637X/779/1/2, 2013.

Rojas Mata, S., Stenberg Wieser, G., Futaana, Y., Bader, A., Persson, M., Fedorov, A., and Zhang, T.: Proton Temperature
425 Anisotropies in the Venus Plasma Environment During Solar Minimum and Maximum, J. Geophys. Res., 127, e2021JA029611, https://doi.org/10.1029/2021JA029611, 2022.

Russell, C. T., Chou, E., Luhmann, J. G., Brace, P. G. L. H., and Hoegy, W. R.: Solar and interplanetary control of the location of the Venus bow shock, J. Geophys. Res., 93, 5461 – 5469, https://doi.org/10.1029/JA093iA06p05461, 1988.

Schmid, D., Volwerk, M., Plaschke, F., Vörös, Z., Zhang, T. L., Baumjohann, W., and Narita, Y.: Mirror mode structures near Venus and
430 Comet P/Halley, Ann. Geophys., 32, 651 – 657, 2014.

Schmid, D., Narita, Y., Plaschke, F., Volwerk, M., Nakamura, R., and Baumjohann, W.: Ion cyclotron waves generated by pick-up protons around Mercury, Geophys. Res. Lett., 48, e2021GL092606, https://doi.org/10.1029/2021GL092606, 2021.

Simon Wedlund, C., Volwerk, M., Mazelle, C., Halekas, J., Rojas-Castillo, D., Espley, J., and Möstl, C.: Making Waves: Mirror Mode Structures Around Mars Observed by the MAVEN Spacecraft, J. Geophys. Res., 127, e2021JA029811, https://doi.org/10.1029/2021JA029811,
435 2022a.

Simon Wedlund, C., Volwerk, M., Mazelle, C., Rojas Mata, S., Stenberg Wieser, G., Futaana, Y., Halekas, J., Espley, J., Rojas-Castillo, D., and Bertucci, C.: Statistical distribution of mirrom mode-like structures in the magnetosheaths of unmagnetized planets: 1. Mars as observed by the MAVEN spacecraft, Ann. Geophys., p. submitted, 2022b.

Sonnerup, B. U. Ö. and Scheible, M.: Minimum and maximum variance analysis, in: Analysis Methods for Multi-Spacecraft Data, edited by
440 Paschmann, G. and Daly, P., pp. 185–220, ESA, Noordwijk, 1998.

Soucek, J., Escoubet, C. P., and Grison, B.: Magnetosheath plasma stability and ULF wave occurrence as a function of location in the magnetosheath and upstream bow shock parameters, J. Geophys. Res., 120, 2838 – 2850, https://doi.org/10.1002/2015JA021087, 2015.

Southwood, D. J. and Kivelson, M. G.: Mirror instability: 1. Physical mechanism of linear instability, J. Geophys. Res., 98, 9181 – 9187, 1993.

445 Svedhem, H., Titov, D. V., McCoy, D., Lebreton, J.-P., Barabash, S., Bertaux, J.-L., Drossart, P., Formisano, V., Häusler, B., Korablev, O., Markiewicz, W. J., Nevejans, D., Pätzold, M., Piccioni, G., Zhang, T. L., Taylor, F. W., Lellouch, E., Koschny, D., Witasse, O., Eggel, H., Warhaut, M., Accomazzo, A., Rodriguez-Canabal, J., Fabrega, J., Schirmann, T., Clochet, A., and Coradini, M.: Venus Express: The first European missionn to Venus, Planet. Space Sci., 55, 1636 – 1652, https://doi.org/10.1016/.pss.2007.01.013, 2007.

Treumann, R. A., Jaroschek, C. H., Constantinescu, O. D., Nakamura, R., Pokhotelov, O. A., and Georgescu, E.: The strange physics of low 450 frequency mirror mode turbulence in the high temperature plasma of the magnetosheath, Nonlin. Proc. Geophys., 11, 647 – 657, 2004.

Tsurutani, B. T., Smith, E. J., Anderson, R. R., Ogilvie, K. W., Scudder, J. D., Baker, D. N., and Bame, S. J.: Lion roars and nonoscillatory drift mirror waves in the magnetosheath, J. Geophys. Res., 87, 6060 – 6072, 1982.

Tsurutani, B. T., Lakhina, G. S., Verkholyadova, O. P., Echer, E., Guarnieri, F. L., Narita, Y., and Constantinescu, D. O.: Magnetosheath and heliosheath mirror mode structures, interplanetary magnetic decreases, and linear magnetic decreases: Differences and distinguishing 455 features, J. Geophys. Res., 116, A02103, 2011.

Volwerk, M., Zhang, T. L., Delva, M., Vörös, Z., Baumjohann, W., and Glassmeier, K.-H.: First identification of mirror mode waves in Venus' magnetosheath?, Geophys. Res. Lett, 35, L12204, https://doi.org/10.1029/2008GL033621, 2008a.

Volwerk, M., Zhang, T. L., Delva, M., Vörös, Z., Baumjohann, W., and Glassmeier, K.-H.: Mirror-mode-like structures in Venus' induced magnetosphere, J. Geophys. Res., 113, E00B16, https://doi.org/10.1029/2008JE003154, 2008b.

460 Volwerk, M., Glassmeier, K.-H., Delva, M., Schmid, D., Koenders, C., Richter, I., and Szegö, K.: A comparison between VEGA 1, 2 and Giotto flybys of comet 1P/Halley: implications for Rosetta, Ann. Geophys., 32, 1441 – 1453, https://doi.org/10.5194/angeo-32-1441-2014, 2014.

Volwerk, M., Schmid, D., Tsurutani, B. T., Delva, M., Plaschke, F., Narita, Y., Zhang, T. L., and Glassmeier, K.-H.: Mirror mode waves in Venus's magnetosheath: solar minimum vs. solar maximum, Ann. Geophys., 34, 1099 – 1108, https://doi.org/10.5194/angeo-34-1099- 465 2016, 2016.

Volwerk, M., Horbury, T. S., Woodham, L. D., Bale, S. D., Simon Wedlund, C., Schmid, D., Allen, R. C., Angelini, V., Bauumjohann, W., Berger, L., Edberg, N. J. T., Evans, V., Hadid, L. Z., Ho, G. C., Khotyaintsev, Y. V., Magnes, W., Maksimovic, M., O'Brien, H., Steller, M. B., Rodriguez-Pacheco, J., and Wimmer-Scheingruber, R. F.: Solar Orbiter's first Venus Flyby: MAG observations of structures and waves associated with the induced Venusian magnetosphere, Astron. Astrophys., 656, A11, https://doi.org/10.1051/0004- 470 6361/202140910, 2021.

Wilson, L. B., Stevens, M. L., Kasper, J. C., Klein, K. G., Maruca, B. A., Bale, S. D., Bowen, T. A., Pulupa, M. P., and Salem, C. S.: The Statistical Properties of Solar Wind Temperature Parameters Near 1 au, Astrophys. J. Suppl. Ser., 236, 41, https://doi.org/10.3847/1538- 4365/aab71c, 2018.

Zhang, T. L., Baumjohann, W., Delva, M., Auster, H.-U., Balogh, A., Russell, C. T., Barabash, S., Balikhin, M., Berghofer, G., Biernat, H. K., 475 Lammer, H., Lichtenegger, H., Magnes, W., Nakamura, R., Penz, T., Schwingenschuh, K., Vörös, Z., Zambelli, W., Fornacon, K.-H., Glassmeier, K.-H., Richter, I., Carr, C., Kudela, K., Shi, J. K., Zhao, H., Motschmann, U., and Lebreton, J.-P.: Magnetic field investigation of the Venus plasma environment: Expected new results, Planet. Space Sci., 54, 1336 – 1343, https://doi.org/10.1016/j.pss.2006.04.018, 2006.

Zhang, T. L., Delva, M., Baumjohann, W., Volwerk, M., Russell, C. T., Barabash, S., Balikhin, M., Pope, S., Glassmeier, K.-H., Kudela,

480   K., Wang, C., Vörös, Z., and Zambelli, W.: Initial Venus express magnetic field observations of the Venus bow shock location at solar
        minimum, Planet. Space Sci., 56, https://doi.org/10.1016/j.pss.2007.09.012, 2008.